ADVANCED BIOMATERIALS

2/09

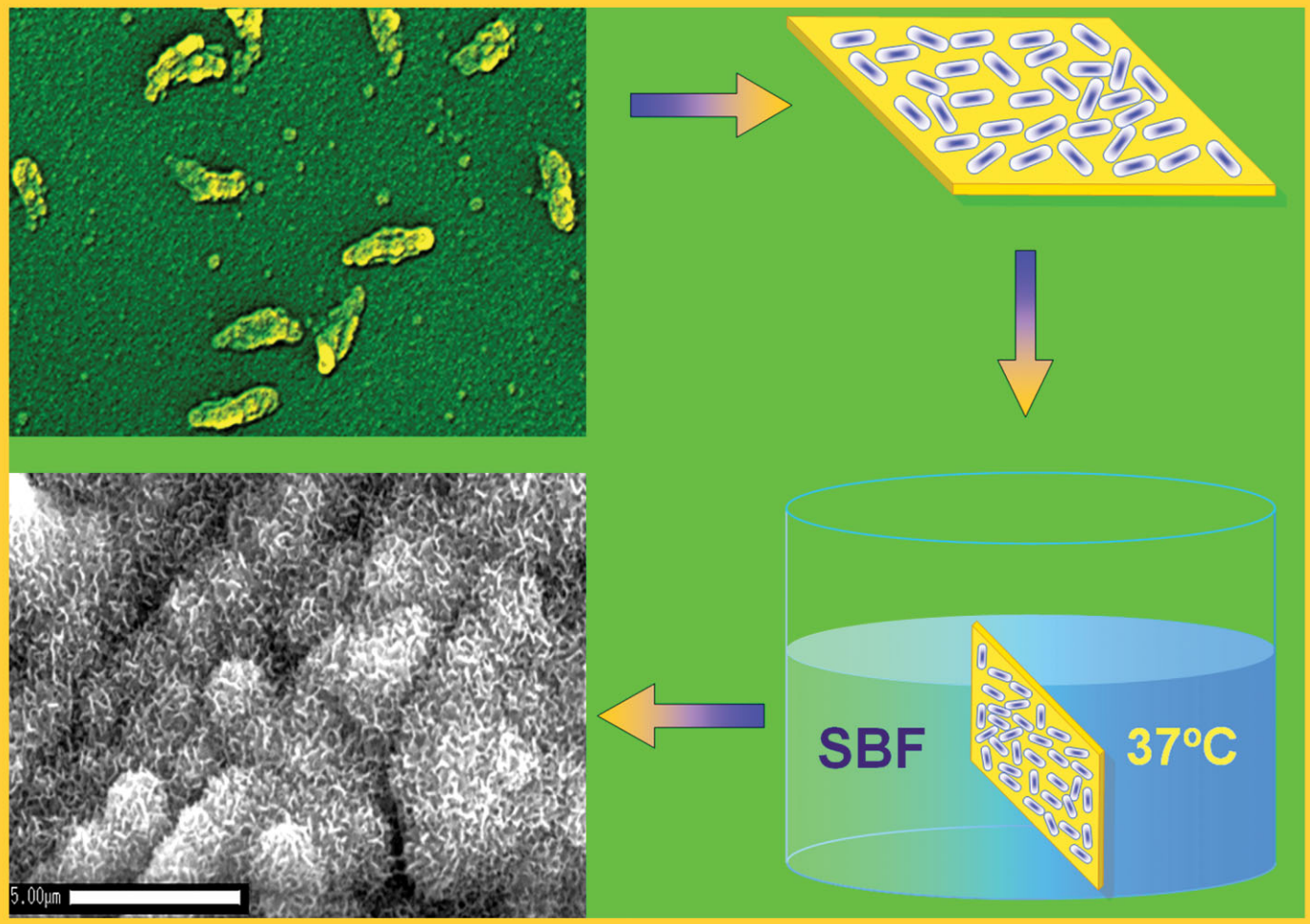

Rice-shaped Bioactive Ceramic Nanoparticles

Poly(D,L-Lactic Acid) Films for in-situ Targeting Gene Transfection

WILEY-VCH

DGM SF2M SVMT

DOI: 10.1002/adem.200800378

Novel Rice-shaped Bioactive Ceramic Nanoparticles**

By *Zhongkui Hong*, Esther G. Merino, Rui L. Reis* and *João F. Mano**

Bioactive glasses/ceramics, such as Bioglass®, which was developed by Hench and Lacefield, are potential materials for bone regeneration and dental applications.[1] Bioactive glass devices implanted at the site of bone defects can directly bond to surrounding tissues by chemical linkage without the formation of a fibrous transitional layer. Compared with hydroxyapatite (HA), bioactive glasses/ceramics exhibit a much higher biomineralization capability *in vitro*, being able to rapidly induce the formation of apatite between the bioactive glass ceramic and a simulated body fluid (SBF). This process involves a complicated ion exchange mechanism between the bioactive glasses and the SBF.[2] In the last five years, a growing consensus has been reached to concentrate on the development of nano-structural bioactive glasses/ceramics materials due to their high biomineralization capability.[3] Bioactive glass/ceramic nanoparticles can be used as strengthening filler in the production of polymer-inorganic nanocomposites.[4] It has also been reported that needle-like or short-fiber inorganic particles can improve the mechanical performance of polymer-inorganic composites much more effectively than spherical fillers.[5] Therefore, an interesting and promising area is the fabrication of nanoparticles with high length-diameter ratios, such as needle-like or rice-shaped particles.

In a previous work, needle-like HA particles have been produced by a coprecipitation method;[6] it was shown that such particles could drastically strengthen the mechanical property of polymer composites. HA has been extensively investigated for several decades, and has been widely applied in bone tissue engineering, general orthopedic applications and clinical dentistry.[7] Bulk HA-based materials can be molded into different shapes to produce implantable devices. HA particles, including nanoparticles, have also been extensively studied. HA particles can be imbedded in polymer matrixes to produce strengthened osteo-conductive porous scaffolds[8] or compact structures for bone fixation.[9] Being the main inorganic component of natural bone, HA exhibits excellent biocompatibility and promotes the attachment and spreading of osteoblasts. However, the ability of HA to induce the formation of an apatite layer on its surface when dipped in simulated body solution (SBF) is relatively low.[10] It has been reported that the incorporation of a small quantity of silicon in the HA lattice can enhance the bioactivity of HA.[11] It has also been reported that the presence of silicon may significantly increase the activity of osteoblast-like cells.[12] *In vivo* testing has also shown a positive result for a silicon-substitute HA (Si-HA) material.[13] Compared with HA ceramics, Si-HA exhibits a remarkably improved new bone formation capability.

The main objective of this study was to synthesize needle-like or rice-shaped bioactive ceramic (BAC) nanoparticles. These were formulated with an unusually low silicon content and a relatively high phosphorus concentration, similar to Si-HA materials. This system may thus combine the advantages of both hydroxyapatite and bioactive glasses, enhancing its potential applicability in regeneration strategies for mineralized tissues or more conventional medical applications. Such nanoparticles can be mixed with some bridgeable polymers to develop new biomaterials with improved mechanical properties and adequate bioactivity.

Experimental

Materials

Tetraethoxysilane [TEOS; $Si(OC_2H_5)_4$, M_w: 208.33, 99.99%], calcium nitrate [$Ca(NO_3)_2 \cdot 4H_2O$, M_w: 236.33, 99%], ammonium dibasic phosphate [$(NH_4)_2HPO_4$, M_w: 132.06, 98%] and citric acid ($C_6H_8O_7$, M_w: 192.123) were obtained from Sigma-Aldrich. Poly(ethylene glycol) (PEG, $\overline{M}_n$: 16 000–24 000) was bought from Fluka. Chitosan (high molecular weight) was also purchased from Sigma-Aldrich, and purified prior to use. All chemicals for polymer purification and preparation of the membrane and the SBF were obtained from Sigma-Aldrich, Germany and used without further purification.

Preparation of Bioactive Ceramic Nano-particles Based on SiO_2-CaO-P_2O_5

BAC [$SiO_2/CaO/P_2O_5 \approx 6:74:20$ (mol)] nanoparticles were prepared using a method based on a procedure previously described.[4b,4c] Briefly, 11.936 g of $Ca(NO_3)_2$ and 0.9063 mL of TEOS were dispersed in a mixture of 60 mL of deionized water

[*] *Dr. Z. Hong, Dr. E. G. Merino, Prof. R. L. Reis, Prof. J. F. Mano*
Bś Research Group – Biomaterials, Biodegradables and Biomimetics, Department of Polymer Engineering
University of Minho, Campus de Gualtar, 4710-057 Braga, (Portugal)
Dr. Z. Hong, Dr. E. G. Merino, Prof. R. L. Reis, Prof. J. F. Mano
IBB – Institute for Biotechnology and Bioengineering, Guimarães, (Portugal)
E-mail: kuihong@gmail.com; jmano@dep.uminho.pt

[**] *This work was financially supported by the Foundation for Science and Technology (FCT) via a grant for postdoctoral research (SFRH/BPD/25828/2005) and by project PTDC/QUI/69263/2006.*

 © 2009 WILEY-VCH Verlag GmbH & Co. KGaA, Weinheim WILEY InterScience DISCOVER SOMETHING GREAT

and 30 mL of ethanol. The pH of the solution was regulated to approximately 2 by adding citric acid, with stirring. After becoming transparent, this solution was dropped into 700 mL of deionized water containing 3.642 g of $(NH_4)_2HPO_4$, with vigorous stirring. During this procedure, the pH of the solution was maintained at approximately 11 by successive addition of an ammonium hydroxide solution. The suspension was stirred at ambient temperature for 24 h, and the precipitate was separated from the reaction mixture by centrifugation at 25 000 rpm, and washed 3 times with deionized water. Then, the white precipitate was suspended in a 2% (w/v) poly(ethylene glycol) solution. The precipitate coated with PEG was freeze-dried (Freezone® 6 L Benchtop Freeze Dry System 7752020, Labconco) at −80 °C and calcinated at 700 °C to obtain the final white BAC nanoparticles.

Field Emission Scanning Electron Microscopy (FESEM)

The morphology of the bioactive nanoparticles was observed using FESEM (XL30 FESEM FEG, Philips) equipped with an energy–dispersive X-ray spectrum (EDS). This microscope was a field emission SEM that allows low-voltage operation and high-resolution observation. The size distribution of nanopowder was calculated from the FESEM images of nanoparticles. The quantitative composition of ceramic powder was roughly assessed by the relative intensity of each element peaks in EDS curve. To avoid the effect of substrate, BAC nanopowder was compressed to 1 mm thick pellets for EDS measurement.

Transmission Electronic Microscope

TEM (JEOL JEM-1011) was used to observe the size and shape of the BAC particles. A typical TEM specimen was prepared by putting a drop of 0.1% (w/v) BAC-water-ethanol suspension onto a carbon-coated copper grid and drying at room temperature in a desiccator.

FTIR Spectroscopic Analysis

A Bio-Rad Win-IR spectrometer was employed for FTIR spectroscopic analysis. The BAC samples were mixed with KBr powder and pressed into a disk suitable for FTIR measurement. The FTIR spectra were recorded from 4 000 to 400 cm^{-1}.

X-ray Diffraction (XRD)

XRD analysis was performed on a X-ray diffractometer (Philips PW 1710, Netherlands) with a Cu-Kα radiation ($\lambda = 0.154$ nm) at 40 kV and 50 mA. Data were collected from $2\theta = 10$ to 60° with a step size of 0.02°. The crystallinity of BAC nanopowder was assessed using the JAD-5 crystalline analysis program.

Chitosan/BAC Membrane Preparation

Chitosan membranes and chitosan membranes containing BAC were prepared by solvent-casting. Acetic acid 2% (w/w) was used to dissolve the polymer to a final concentration of 1% (w/v). The chitosan solution was agitated constantly for 1 day and filtered to remove impurities. For the composite membranes, a given quantity of nanoparticles (20 wt.-%) was added to the polymer solution. This mixture was stirred for 2 h and then sonicated for 15 min. The final solution was poured into plastic Petri dishes (120×120 mm^2) and left to dry at room temperature for 10 days. After drying, the prepared composite membranes were neutralised in 0.1 M sodium hydroxide solution for 10 min, washed several times with distilled water and left to dry at room temperature for 1 day. Chitosan membranes without the inorganic component were also prepared to be used as a control.

In Vitro Bioactivity Test

For the *in vitro* bioactivity tests, an acellular 1.0× SBF was prepared in accordance with the formulation described by Kokubo and co-workers [14]. Sample membranes of 20×15 mm^2 were cut from the original processed films for the bioactivity tests. Three replicates for each sample were immersed in SBF for 7 days at 37 °C. After being removed from the SBF, the sample membranes were gently rinsed with distilled water and dried at room temperature.

Scanning Electron Microscopy (SEM)

The morphological analysis of these membranes was performed using SEM (Leica Cambridge S 360) at an accelerated voltage of 15 kV. Before being observed by SEM, the membranes were gold coated using a Hitachi coating unit IB-2 coater at 6 mA. The Ca and P elements were identified by energy dispersive spectroscopy (EDS, Oxford Link eXLII); for this elemental characterization the membranes had to be carbon coated.

Results and Discussion

Morphology and Composition of BAC Nanoparticles

Figure 1a and b show a representative FESEM image and the corresponding EDS curve of BAC nanoparticles prepared in this work. Most of the particles exhibit a rice-like shape and a very rough surface, which results from the assembly of 20 nm sized spherical nanoparticles. Such a coarse surface tends to increase the specific surface area of the BAC powder. Mixed with biodegradable or biocompatible polymers, it could provide a more reactive and adsorptive interface between the polymer component and the BAC filler. The EDS curve indicates the existence of a small amount of carbon and silicon in the BAC nanoparticles.

The approximate composition of BAC taken from the curve is $SiO_2/CaO/P_2O_5 \approx 6.3{:}71{:}22.7$ (mol), which is a slight deviation from the precursors formulation of $Si/Ca/P_2O_5 \approx 6{:}74{:}20$ (mol). The content of calcium was lower than in the initial reaction mixture, which mainly resulted from the removal of free Ca^{2+} that was not fully incorporated in the silica or phosphoric gel network during the washing procedure. In this kind of BAC nanoparticles, the ratio of Ca to P was 1.564, which is lower than stoichiometric HA in

 © 2009 WILEY-VCH Verlag GmbH & Co. KGaA, Weinheim

ADVANCED ENGINEERING MATERIALS

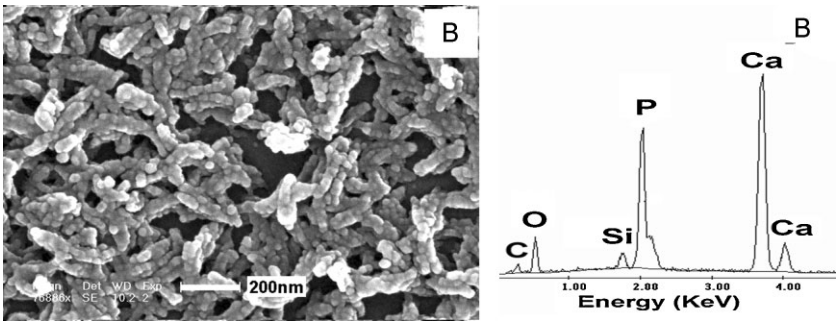

Fig. 1. a) FESEM image and b) EDX curve of the prepared BAC powder. $SiO_2/CaO/P_2O_5 \approx 6.3:71:22.7$ (mol); Ca: P ≈ 1.564 (mol).

the composition of natural bone; therefore, it is a calcium-deficient material.

Figure 2a shows the excellent dispersibility of the BAC nanoparticles, indicating that the system may be effectively suspended in water-ethanol mixtures. Generally, the agglomeration of nanoparticles takes place in the step of condensation or drying of gel particles. In order to avoid the aggregation of nanoparticles, an extremely diluted reaction solution was used for condensation of gel particle, and subsequently subjected to lyophilization for drying of gel particles.

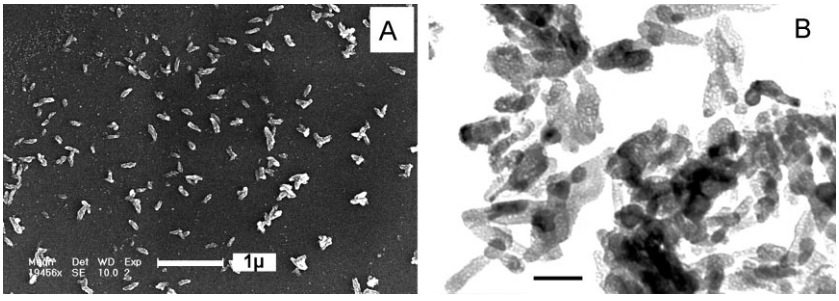

Fig. 2. a) FESEM image of BAC nanoparticles dispersed in ethanol-water solution. b) TEM image of BAC nanoparticles; the bar is 100 nm.

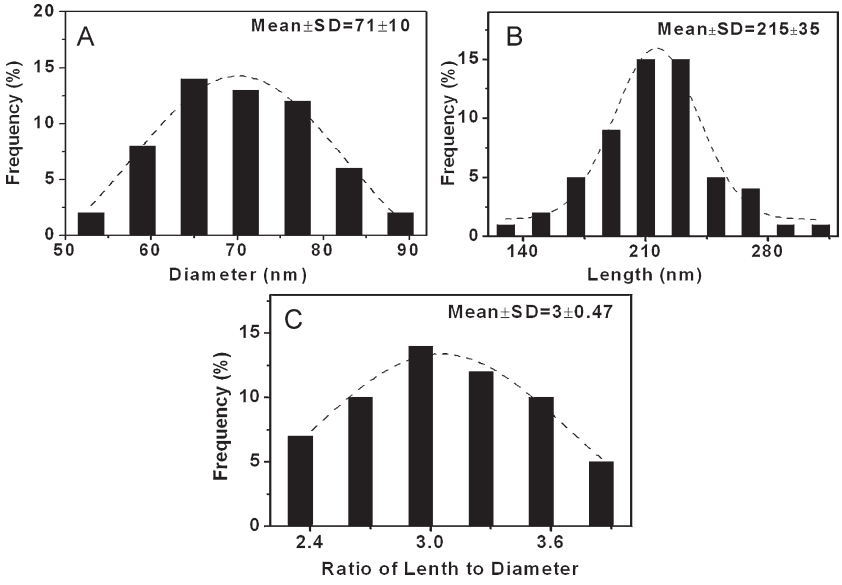

Fig. 3. Size distribution of BAC nanoparticle powder: a) diameter, b) length, and, c) length to diameter ratio. Solid curves are Gaussian fits to the histograms.

A TEM image of the BAC nanopowder is shown in Figure 2b. A mesoporous structure can be seen by examining the image of a single particle. In terms of mechanism, our hypothesis is under freezing, gel particles can maintain their initial shape and size, resulting in phase separation between calcium phosphate-silicate gel network and the water-ethanol solution absorbed in the gel particles. Furthermore, during lyophilization the gel network cannot shrink along with the extraction of water and ethanol. Therefore, after drying and calcination, some nanometric-size voids are formed in regions previously occupied by water, ethanol, and organic precursors. This mesoporous structure would increase the specific surface area of BAC nanopowder and could possibly stimulate the biomineralization process.[3d,6]

Before being subjected to lyophilization, gel particles were enveloped with a compact PEG thin coating by strong hydrogen bonds formed between the surface hydroxyls of the gel particles and the surfactant molecules. PEG surfactant may effectively reduce the interparticle collision that can result in the interaction of surface hydroxyl of gel particles and aggregation of BAC nanoparticles.

The size distribution of the BAC nanoparticles is quite narrow, as shown in Figure 3. Most of the particles are around 70 nm in diameter and 215 nm in length. The length/diameter ratio mostly ranges between 2.3 and 3.8. The presence of silicon in the formulation did not change the growth tendency of HA particles along the C-axis. The morphology of the new BAC nanoparticles is similar to HA nanoparticles prepared previously by a coprecipitation route.[6] If incorporated into polymer matrixes, such anisotropic nanoparticles could effectively strengthen the composite material, compared to spherical fillers.

XRD and FTIR

The XRD curves of both BAC and HA particles exhibit similar characteristics, with the typical HA diffraction peaks being seen at $2\theta = 26$ and 32° in both cases (see Figure 4). However, the reflections for BAC are broader than those of HA and some small crystalline peaks disappeared in the BAC's XRD pattern. With the introduction of the silicon component, crystallinity was slightly decreased to approximately 95%, as estimated by JAD-5 analysis from the XRD curve. This indicates that the silicon component imbedded in the

 © 2009 WILEY-VCH Verlag GmbH & Co. KGaA, Weinheim

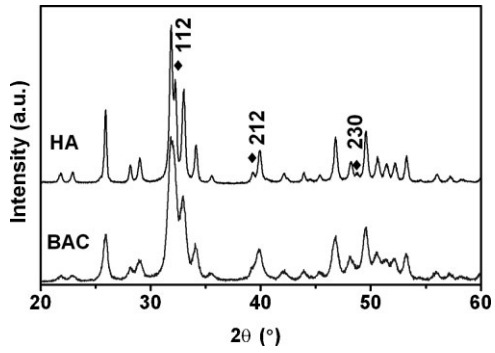

Fig. 4. XRD pattern of the BAC powder and HA powder. (HA powder was prepared by the sol-gel method with $Ca(NO_3)_2$ and $(NH_3)_2HNO_3$ under alkaline condition.)

phosphate lattice disturbed the crystallization, when compared with HA.

The changes in the XRD pattern could be attributed to the formation of hydroxyl vacancies, resulting from the substitution of phosphates by silicates. The differences could be also ascribed to the change in the crystal sizes. Some researchers believe that, in this kind of ceramic material, silicon is not incorporated in the calcium phosphate gel network to substitute the phosphorous in the gel structure.[13,15] In the sol-gel process, the silicon precursor might be hydrolyzed to a silica gel and calcined to a silicon dioxide phase in the final ceramic particle. Another possibility is that hydrolyzed silicon sol might have coprecipitated with calcium ions to form a calcium silicate minor phase, which coexisted with the major phase of phosphate.

The FTIR spectrum of the BAC particles is presented in Figure 5a. The typical FTIR spectrum of HA powder is also given here for comparison. The wide absorption bands at 3 433 and 1 630 cm^{-1} should be assigned to the stretching vibration of the H–O bond of a small quantity of H_2O that was absorbed in the ceramic powders. The intense stretching vibration band of PO_4^{3-} appears at 1 093, 1 037 and 960 cm^{-1}. The sharp double peaks at 601 and 564 cm^{-1} correspond to the O–P–O ν_4 bending mode. The small peak at 625 cm^{-1} was associated with the liberation mode of O–H.[16] The stretching vibration band of Si–O should appear between 1 100 and 1 000 cm^{-1}, but it was overlapped by the stretching vibration band of P–O. It should also be noted that the carbonate absorption bands at 1 446, 1 414, and 875 cm^{-1} appeared in both spectra. The carbonate existing in the lattice of the BAC powders could be the result of the dissolution of CO_2 from the atmosphere during the sol-gel procedure. The assignment of the peak at 875 cm^{-1} is not straightforward. Some researcher attributed it to the HPO_4^{2-} group,[17] while it was also identified as the ν_3 Si–O stretching band in the silicate lattice.[18]

Figure 5b extends the FTIR spectra between 800 and 1 000 cm^{-1}. A new absorption band is observed at 925 cm^{-1}, which has been considered as evidence of the incorporation of silicon in the phosphate structure.[17b,19] The slight increase in the 875 cm^{-1} peak should be attributed to the overlapping of the silicate, phosphate, and carbonate bands.

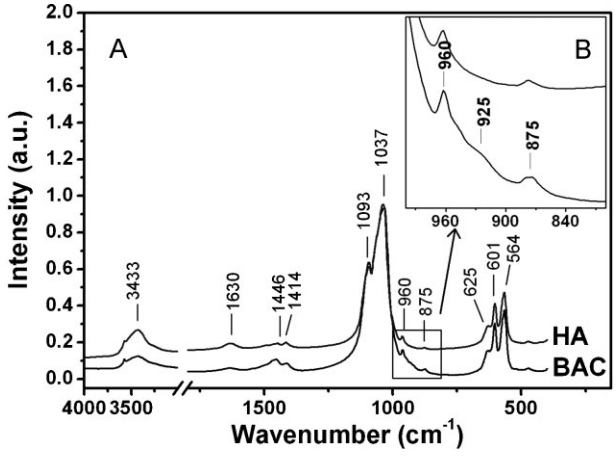

Fig. 5. a) FTIR spectrum of the BAC powder between 400 and 4 000 cm^{-1}. b) Extended FTIR spectrum of BAC nanoparticles between 800 and 1 000 cm^{-1}. The FTIR spectrum of HA is shown for comparison.

In Vitro Bioactivity Test

The results of the bioactivity test obtained in both chitosan and chitosan/inorganic composite membranes were evaluated using SEM and EDS. After an immersion period of 7 days in SBF at 37 °C, the SEM results in the composite membrane showed the presence of an apatite layer with a cauliflower-like morphology resulting from the assembly of nano-size needle-like ceramic crystals (Figure 6a). This precipitate consisted of the typical bone-like apatite coating that is produced onto osteoconductive materials upon *in vitro* bioactivity tests. The EDS test confirms the presence of calcium and phosphorous in this ceramic layer (Figure 6b). As expected, no apatite was formed in the unfilled chitosan membranes, as shown in the SEM image and EDS curve (Figure 6c and d, respectively) of pure chitosan film.

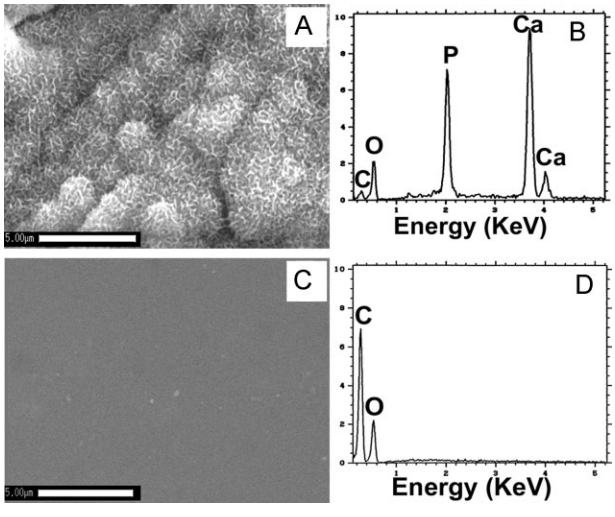

Fig. 6. a) SEM image of the apatite layer formed on the chitosan/BAC composite membrane after 7 days of immersion in SBF, and, b) corresponding EDS results obtained from analysis of the same sample. c) SEM image, and, d) EDS curve of neat chitosan film after 7 days of immersion in SBF, shown for comparison. The bar is 5 μm

 © 2009 WILEY-VCH Verlag GmbH & Co. KGaA, Weinheim

ADVANCED ENGINEERING MATERIALS

Conclusions

New rice-shaped or claviform low-silicon-content bioceramic nanoparticles were produced by an improved sol-gel method, with sizes of about 70 nm in diameter and 210 nm in length. Calcination at 700 °C did not destroy the global protuberances on the surface of the nanoparticles. Such a coarse texture can improve the specific surface area of nano-particles, facilitate the resolvability of the BAC material and, consequently, increasing its bioactivity. If combined with biocompatible polymers, the rough surface of the nanofiller, combined with its anisotropy, would favor an increase in the strength of the composite material. *In vitro* bioactivity tests showed that these novel bioactive nanoparticles, containing small quantity of silicon, have excellent biomineralization capability. The results of this study suggest that such new nanoparticulate systems could find applications in orthopedic-replacement-based strategies or be introduced in scaffolds for bone tissue engineering.

Received: November 3, 2008
Final Version: January 16, 2009

[1] W. R. Lacefield, L. L. Hench, *Biomaterials* **1986**, *7*, 104.
[2] P. Saravanapavan, J. R. Jones, R. S. Pryce, L. L. Hench, *J. Biomed. Mater. Res.* **2003**, *66A*, 110.
[3] a) Q. Shi, J. Wang, J. Zhang, J. Fan, G. D. Stucky, *Adv. Mater.* **2006**, *18*, 1038. b) T. A. Ostomel, Q. Shi, C. K. Tsung, H. Liang, G. D. Stucky, *Small* **2006**, *2*, 1261. c) T. A. Ostomel, Q. Shi, G. D. Stucky, *J. Am. Chem. Soc.* **2006**, *128*, 8384. d) X. Yan, C. Yu, X. Zhou, J. Tang, D. Zhao, *Angew. Chem.* **2004**, *116*, 5753.
[4] a) A. Liu, Z. Hong, X. Zhuang, X. Chen, Y. Cui, Y. Liu, X. Jing, *Acta Biomater.* **2008**, *4*, 1005. b) Z. Hong, R. L. Reis, J. F. Mano, *J. Biomed. Mater. Res.* **2009**, *88A*, 304. c) Z. Hong, R. L. Reis, J. F. Mano, *Acta Biomater.* **2008**, *4*, 1297. d) S. Ghosh, R. L. Reis, J. F. Mano, *Adv. Biomater.* **2008**, B18–B22. DOI: 10.1002/adem.200700360.
[5] a) K. McGrath, D. Kaplan, in *Protein-based Materials*, (Eds: Birkhäuser), Springer, **1996**, p. 185. b) S. Du, Y. Tian, J. Liu, H. Liu, Y. Chen, *Mater. Lett.* **2006**, *60*, 3133. c) H. Unal, A. Mimaroglu, M. Alkan, *Polym. Int.* **2004**, *53*, 56.
[6] Z Hong, P. Zhang, A. Liu, L. Chen, X. Chen, X. Jing, *J. Biomed. Mater. Res.* **2007**, *81A*, 515.
[7] a) L. L. Hench, *J. Am. Ceram. Soc.* **1991**, *74*, 1487. b) K. Yamagishi, K. Onuma, T. Suzuki, F. Okada, J. Tagami, M. Otsuki, P. Senawangse, *Nature* **2005**, *433*, 819. c) L. L. Hench, J. M. Polak, *Science* **2002**, *295*, 1014. d) P. Ducheyne, Q. Qiu, *Biomaterials* **1999**, *20*, 2287. f) W. Suchanek, M. Yoshimura, *J. Mater. Res.* **1998**, *13*, 94.
[8] a) A. P. Marques, R. L. Reis, J. A. Hunt, *Biomaterials* **2002**, *23*, 1471. b) G. Wei, P. X. Ma, *Biomaterials* **2004**, *25*, 4749. c) J. Sundaram, T. D. Durance, R. Wang, *Acta Biomater.* **2008**, *4*, 932.
[9] a) Y. Shikinami, M. Okuno, *Biomaterials* **1999**, *20*, 859. b) Y. Shikinami, M. Okuno, *Biomaterials* **2001**, *22*, 3197.
[10] a) I. D. Xynos, M. V. J. Hukkanen, L. D. K. Buttery, L. L. Hench, J. M. Polak, *Calcif. Tissue Int.* **2000**, *67*, 321. b) D. L. Wheeler, M. J. Montfort, S. W. McLoughlin, *J. Biomed. Mater. Res.* **2001**, *55A*, 603.
[11] A. E. Porter, N. Patel, J. N. Skepper, S. M. Best, W. Bonfield, *Biomaterials* **2003**, *24*, 4609.
[12] E. S. Thian, J. Huang, S. M. Best, Z. H. Barber, W. Bonfield, *Mater. Sci. Eng.* **2007**, *27C*, 251.
[13] C. L. Camiré, S. J. Saint-Jean, C. Mochales, P. Nevsten, J. S. Wang, L. Lidgren, I. McCarthy, M. P. Ginebra, *J. Biomed. Mater. Res.* **2006**, *76B*, 424.
[14] T. Kokubo, H. Takadama, *Biomaterials* **2006**, *27*, 2907.
[15] M. W. Barnes, M. Klimkiewicz, P. W. Brown, *J. Am. Ceram. Soc.* **1992**, *76*, 1423.
[16] S. Sprio, A. Tampieri, E. Landi, M. Sandri, S. Martorana, G. Celotti, G. Logroscino, *Mater. Sci. Eng.* **2008**, *28C*, 179.
[17] a) J. W. Reida, L. Tuck, M. Sayer, K. Fargo, J. A. Hendry, *Biomaterials* **2006**, *27*, 2916. b) I. R. Gibson, S. M. Best, W. Bonfield, *J. Biomed. Mater. Res.* **1999**, *44*, 422.
[18] D. Arcos, J. Rodríguez-Carvajal, M. Vallet-Regí, *Chem. Mater.* **2005**, *17*, 57.
[19] a) A. R. Boccaccini, Q. Chen, L. Lefebvre, L. Gremillard, J. Chevalier, *Faraday Discuss.* **2007**, *136*, 27. b) Th. Leventouri, C. E. Bunaciu, V. Perdikatsis, *Biomaterials* **2003**, *24*, 4205.

 © 2009 WILEY-VCH Verlag GmbH & Co. KGaA, Weinheim